Journal of Molecular Structure 1319 (2025) 139519

Contents lists available at ScienceDirect

Journal of Molecular Structure

journal homepage: www.elsevier.com/locate/molstr

# Exploring highly selective polymethoxy fenamate isosteres as novel anti-prostate cancer agents: Synthesis, biological activity, molecular docking, molecular dynamics, and ADME studies

Feyzi Sinan Tokalı [a,*], Halil Şenol [b,*], Şeyma Ateşoğlu [c,d], Pelin Tokalı [e], Fahri Akbaş [d]

[a] Department of Material and Material Processing Technologies, Kars Vocational School, Kafkas University 36100 Kars, Türkiye
[b] Department of Pharmaceutical Chemistry, Faculty of Pharmacy, Bezmialem Vakif University 34093 Fatih, Istanbul, Türkiye
[c] Department of Biotechnology, Institute of Health Sciences, Bezmialem Vakif University 34093 Fatih, Istanbul, Türkiye
[d] Department of Medical Biology, Faculty of Medicine, Bezmialem Vakif University 34093 Fatih, Istanbul, Türkiye
[e] Department of Veterinary Physiology, Faculty of Veterinary Medicine, Kafkas University 36100, Kars, Türkiye

ARTICLE INFO

*Keywords:*
Hydrazone
Prostate cancer
Cytotoxicity
Molecular docking
Molecular dynamics

ABSTRACT

In this study, we synthesized and characterized sixteen new polymethoxy-substituted hydrazone derivatives. These compounds were evaluated for their *in vitro* cytotoxic activity against human prostate cancer (PC3) and human umbilical vein endothelial (HUVEC) cell lines. Compounds **5, 6, 7,** and **11** exhibited significant cytotoxic effects with high selectivity index. Molecular docking studies and MM-GBSA binding free energy calculations were performed against tubulin protein. Compound **7** emerged as a particularly promising candidate, displaying an $IC_{50}$ value of 1.49 μM against PC3 cells and a selectivity index of 264. Compound **7** achieved impressive docking score -13.655 kcal/mol against tubulin and formed stable hydrogen bonds and π-π stacking interactions with key residues in this protein. MD simulations confirmed the stability of the **7-tubulin** complex. ADME analysis indicated that compound **7** has favorable absorption, solubility, and permeability properties, with minimal rule violations. The SAR analysis highlighted the significance of specific functional groups in enhancing the compound's cytotoxic and binding properties. Overall, compound **7** is identified as a leading candidate due to its exceptional cytotoxicity, high selectivity index, strong binding affinities, and favorable pharmacokinetic profile, making it a top candidate for further investigation and development as a novel anticancer agent.

## 1. Introduction

Cancer, characterized by the uncontrolled increase in cell growth and proliferation due to disruption of the mechanisms controlling cell growth and/or genetic mutations, is one of the leading causes of death worldwide. Despite this, there have been significant advancements in its treatment, leading to improved outcomes and survival rates for many patients [1]. According to the previously reported studies approximately 19 million people worldwide were affected by various types of cancer and approximately 10 million people died due to cancer.

Prostate cancer (PCa) is one of the most common cancers in men nowadays [2]. The prostate gland is an androgen-dependent organ, and PCa is originally dependent on androgen receptor for growth and survival [3,4]. Therefore, inhibiting the enzymes that play an important role in the biosynthesis of androgen is a promising approach for the treatment of prostate cancer [5]. While prostate cancer is 7.3 % among cancer types, this rate is 14.1 % when evaluated only in terms of male patients. When evaluated in terms of mortality, 6.8 % of men who died due to cancer were shown to be due to prostate cancer [6].

Tubulin, a protein forming microtubules critical for cell division, shape, and transport, influences cancer by disrupting these processes. It plays a vital role in mitosis, aiding cell division, and drugs targeting tubulin-associated microtubules inhibit cancer cell proliferation. Moreover, microtubules impact cancer cell migration crucial for metastasis [7,8]. Tubulin plays a significant role in the treatment and understanding of prostate cancer. In prostate cancer, targeting tubulin can disrupt these processes, leading to cancer cell death. Inhibition of tubulin polymerization is one of the current approaches in the design of anticancer agents. There are many studies reporting the anticancer properties of polymethoxy substituted chalcones [9,10], quinoline and

* Corresponding authors.
*E-mail addresses:* feyzitokali@kafkas.edu.tr (F.S. Tokalı), hsenol@bezmialem.edu.tr (H. Şenol).

https://doi.org/10.1016/j.molstruc.2024.139519
Received 25 June 2024; Received in revised form 12 July 2024; Accepted 30 July 2024
Available online 2 August 2024

quinazolines [11,12], indoles [13], oxadiazoles [14], triazoles [15], benzofurans [16], and pyrrolizines [17].

Methoxy or polymethoxy substituted compounds represent an important class frequently used in drug design today. It is known that polymethoxy substituted compounds from various compound classes have antioxidant [18], anti-inflammatory and anti-colitis [19], antimicrobial and antifungal [20], antitumor [21], antimitotic [22] properties. In addition to these properties of polymethoxy compounds, the main application area is the design and discovery studies of anticancer agents. They show anticancer activity mostly by inhibiting tubulin polymerization. On the other hand, the hydrazide-hydrazone or arylidenehydrazide pharmacophore is a functional group with many activities such as anticancer [23-25], antimicrobial [26,27], antimycobacterial [28], antioxidant [29,30], anticholinergic [31], antidiabetic [32].

This study aims to synthesize of new series of polymethoxy-substituted hydrazone compounds based on anthranilic acid to investigate their inhibitory effects on prostate cancer cells and evaluate the possible inhibition mechanisms. Additionally, it will examine the *in vitro* and *in silico* biological activities of these compounds, along with their estimated ADME parameters and drug similarities.

## 2. Results and discussion

### 2.1. Chemistry

In this study, sixteen new methoxy substituted hydrazone derivatives were synthesized. The hydrazides **(1–4)** were synthesized as the starting materials by using methyl anthranilate or 4,5-dimethoxy methyl anthranilate according to the method reported previously [33]. The target polymethoxy substituted hydrazone compounds **(5–20)** were obtained in excellent yields (98–94 %) from the reactions of compounds **1–4** with various methoxy substituted benzaldehydes such as 2,6-dimethoxy benzaldehyde, 3,4-dimethoxy benzaldehyde, syringaldehyde, and 3,4,5-trimethoxy benzaldehyde (Scheme 1). The R groups of the synthesized compounds are clearly presented in Table 1. The structures of the target compounds were characterized by FTIR, $^{1}$H NMR, $^{13}$C NMR (APT), and HRMS spectroscopic techniques.

In the FTIR spectra of the compounds **5–20**, the stretching bands of amide and hydrazide NH are observed at 3271 – 3169 cm$^{-1}$. Aromatic C–H stretching bands are observed at 3083 – 3052 cm$^{-1}$. C = O stretching bands of the hydrazide and amide moieties are observed at 1683 – 1657 cm$^{-1}$ and 1653 – 1628 cm$^{-1}$, respectively. Finally, the characteristic N=CH stretching bands are observed at 1610 – 1582 cm$^{-1}$ [34].

In the $^{1}$H NMR spectra of compounds **5–20**, peaks of amide and hydrazide NH protons appeared as broad singlet at δ 12.42 – 11.97 ppm and δ 11.92 – 11.59 ppm, respectively. Phenolic OH protons of compounds **7, 11, 15**, and **19** are observed as a singlet at δ 9.00 – 8.97 ppm. Peaks of N=CH protons resonated as a singlet at δ 8.81 – 8.35 ppm. Aromatic protons are observed at δ 8.58 – 6.99 ppm as doublet, triplet and multiplet relative to their chemical environment. Peaks of the all methoxy protons are observed at δ 3.96 – 3.72 ppm [34,35].

In the $^{13}$C NMR spectra of compounds **5–20**, peaks of C = O carbons of hydrazide and amide moieties are observed at δ 165.4 – 164.5 ppm. Peaks of CH=N carbons appeared at δ 150.1 – 144.1 ppm. Peaks of aromatic carbons resonated at δ 162.7 – 104.5 ppm. Peak of the all $OCH_3$ carbons appeared at δ 60.6 – 55.8 ppm [34,35].

### 2.2. Biological activity studies

To evaluate *in vitro* cytotoxic activity of synthesized compounds, they were tested against human prostate cancer cell (PC3) and human umbilical vein endothelial cell (HUVEC) lines. Doxorubicin (dox) and temozolomide (tmz) were used as reference inhibitors and results are given in Table 2**.** The inhibition graphs can be seen in Supporting Information (SI) file.

Compounds **5, 6, 7,** and **11** emerge as highly promising candidates based on their *in vitro* cytotoxic effects against HUVEC and PC3 cell lines. Compound **5** exhibits a potent inhibition of cancer cell growth with an $IC_{50}$ of 1.48 μM for PC3 and a noteworthy selectivity index (SI) of 199, highlighting its substantial specificity for cancer cells. Similarly, compound **6** displays impressive potency against PC3 with an $IC_{50}$ of 1.98 μM and a high SI of 115. Compound **7** stands out with a most potent $IC_{50}$ of 1.49 μM for PC3 and an outstanding SI of 264.4, emphasizing its remarkable selectivity for cancer cells. Compound **11** demonstrates notable potency with an $IC_{50}$ of 3.70 μM for PC3 and a high SI of 45. These four compounds not only exhibit lower $IC_{50}$ values for cancer cells compared to normal cells but also boast higher selectivity index than established reference drugs doxorubicin and temozolomide. On the other hand, several compounds exhibit a moderate range of potencies against PC3 cell lines, with some demonstrating notable $IC_{50}$ values. Additionally, all the synthesized compounds are safer than doxorubicin and temozolomide when tested against the HUVEC cell line. While all of the compounds synthesized in this study are more selective than doxorubicin, only the selectivities of compounds **9, 10** and **12** have lower than temozolomide. Although temozolomide and doxorubicin show high inhibitory activity against PC3 cells, their selectivity is lower than the synthesized compounds due to their toxic effects on healthy cells. In this study, compounds **5, 6, 7** and **11,** which stand out both for their high inhibitory effectiveness against PC3 cells and their low toxicity on healthy cells, are safer and more potent than the reference drugs. As conclusion, with an $IC_{50}$ of 1.49 μM for PC3 and an exceptional SI of 264.4, compound **7** showcases remarkable potency and selectivity for cancer cells. This compound not only surpasses the efficacy of reference drugs doxorubicin and temozolomide but also demonstrates a superior selectivity profile. Its high SI indicates a significant ability to discriminate between cancer and normal cells, a crucial aspect for the development of safe and effective anticancer agents. Additionally, compound **7**′s potency, as evidenced by its low $IC_{50}$ for PC3, positions it as a frontrunner for further investigation.

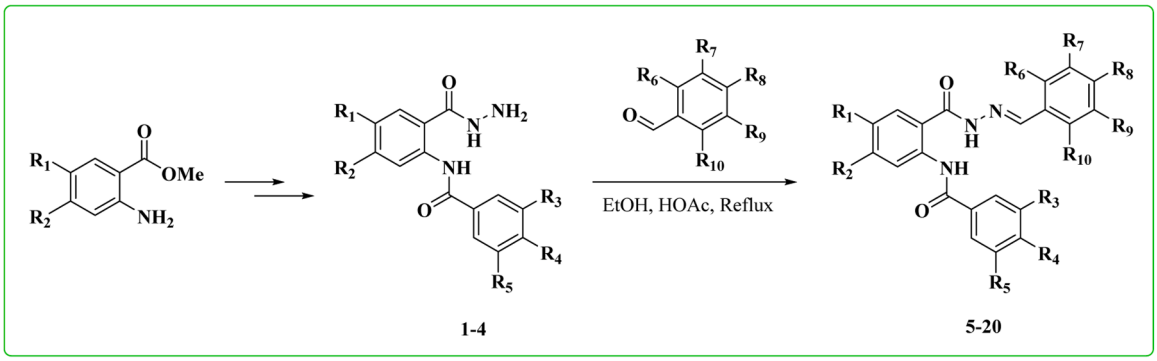


**Scheme 1.** Synthesis of compounds **5–20**.

**Table 1**
The R groups in synthesized compounds **1–20**.

| Compounds | $R_1$ | $R_2$ | $R_3$ | $R_4$ | $R_5$ | $R_6$ | $R_7$ | $R_8$ | $R_9$ | $R_{10}$ |
|---|---|---|---|---|---|---|---|---|---|---|
| **1** | H | H | H | $OCH_3$ | H | – | – | – | – | – |
| **2** | H | H | $OCH_3$ | $OCH_3$ | $OCH_3$ | – | – | – | – | – |
| **3** | $OCH_3$ | $OCH_3$ | H | $OCH_3$ | H | – | – | – | – | – |
| **4** | $OCH_3$ | $OCH_3$ | $OCH_3$ | $OCH_3$ | $OCH_3$ | – | – | – | – | – |
| **5** | H | H | H | $OCH_3$ | H | $OCH_3$ | H | H | H | $OCH_3$ |
| **6** | H | H | H | $OCH_3$ | H | H | H | $OCH_3$ | $OCH_3$ | H |
| **7** | H | H | H | $OCH_3$ | H | H | $OCH_3$ | OH | $OCH_3$ | H |
| **8** | H | H | H | $OCH_3$ | H | H | $OCH_3$ | $OCH_3$ | $OCH_3$ | H |
| **9** | H | H | $OCH_3$ | $OCH_3$ | $OCH_3$ | $OCH_3$ | H | H | H | $OCH_3$ |
| **10** | H | H | $OCH_3$ | $OCH_3$ | $OCH_3$ | H | H | $OCH_3$ | $OCH_3$ | H |
| **11** | H | H | $OCH_3$ | $OCH_3$ | $OCH_3$ | H | $OCH_3$ | OH | $OCH_3$ | H |
| **12** | H | H | $OCH_3$ | $OCH_3$ | $OCH_3$ | H | $OCH_3$ | $OCH_3$ | $OCH_3$ | H |
| **13** | $OCH_3$ | $OCH_3$ | H | $OCH_3$ | H | $OCH_3$ | H | H | H | $OCH_3$ |
| **14** | $OCH_3$ | $OCH_3$ | H | $OCH_3$ | H | H | H | $OCH_3$ | $OCH_3$ | H |
| **15** | $OCH_3$ | $OCH_3$ | H | $OCH_3$ | H | H | $OCH_3$ | OH | $OCH_3$ | H |
| **16** | $OCH_3$ | $OCH_3$ | H | $OCH_3$ | H | H | $OCH_3$ | $OCH_3$ | $OCH_3$ | H |
| **17** | $OCH_3$ | $OCH_3$ | $OCH_3$ | $OCH_3$ | $OCH_3$ | $OCH_3$ | H | H | H | $OCH_3$ |
| **18** | $OCH_3$ | $OCH_3$ | $OCH_3$ | $OCH_3$ | $OCH_3$ | H | H | $OCH_3$ | $OCH_3$ | H |
| **19** | $OCH_3$ | $OCH_3$ | $OCH_3$ | $OCH_3$ | $OCH_3$ | H | $OCH_3$ | OH | $OCH_3$ | H |
| **20** | $OCH_3$ | $OCH_3$ | $OCH_3$ | $OCH_3$ | $OCH_3$ | H | $OCH_3$ | $OCH_3$ | $OCH_3$ | H |

**Table 2**
*In vitro* cytotoxic effects and selectivity index of target molecules against HUVEC and PC3 cell lines.

| | $IC_{50}$ (μM) | | Selectivity Index (SI) |
|---|---|---|---|
| Compounds | HUVEC | PC3 | HUVEC/PC3 |
| **5** | 295.20 ± 4.12 | 1.48 ± 0.12 | 199.5 |
| **6** | 228.20 ± 3.43 | 1.98 ± 0.13 | 115.2 |
| **7** | 394.00 ± 5.22 | 1.49 ± 0.11 | 264.4 |
| **8** | 339.60 ± 5.18 | 15.76 ± 0.45 | 21.5 |
| **9** | 146.70 ± 2.46 | 28.68 ± 0.86 | 5.1 |
| **10** | 138.50 ± 2.32 | 31.28 ± 0.92 | 4.4 |
| **11** | 167.10 ± 2.86 | 3.70 ± 0.17 | 45.1 |
| **12** | 70.35 ± 1.79 | 20.52 ± 0.98 | 3.4 |
| **13** | 123.1 ± 2.12 | 5.45 ± 0.25 | 22.5 |
| **14** | 174.4 ± 2.59 | 9.94 ± 0.44 | 17.5 |
| **15** | 254.7 ± 3.41 | 13.74 ± 0.52 | 18.5 |
| **16** | 272.4 ± 3.78 | 20.94 ± 0.88 | 13.0 |
| **17** | 322.1 ± 4.12 | 16.91 ± 0.71 | 19.0 |
| **18** | 290.7 ± 3.76 | 26.78 ± 0.54 | 10.8 |
| **19** | 292.5 ± 3.22 | 18.79 ± 0.32 | 15.5 |
| **20** | 236.5 ± 2.88 | 25.71 ± 0.43 | 9.2 |
| **Doxorubicin** | 9.06 ± 0.43 | 5.20 ± 0.21 | 1.7 |
| **Temozolomide** | 13.88 ± 0.88 | 2.12 ± 0.09 | 6.5 |

### 2.3. Molecular docking

Molecular docking is a powerful computational technique that accelerates the drug discovery process by predicting and optimizing the interactions between potential drug candidates and their target proteins. Its integration into the drug development pipeline enhances efficiency, reduces costs, and contributes significantly to the identification and development of novel therapeutic agents [36].

In this study the induced fit docking (IFD) protocol was used for molecular docking studies. In addition, MM-GBSA (Molecular Mechanics Generalized Born Surface Area) ΔG binding free energies of compounds were calculated to determine ligand protein binding affinity. IFD accounts for protein flexibility by allowing both the ligand and the protein receptor to adapt to each other's shape, resulting in more accurate binding predictions. On the other hand, MM-GBSA calculates the free energy of binding by combining molecular mechanics force field calculations with generalized born solvent models, providing insights into the stability of ligand-protein interactions. Together, these methods enhance our understanding of molecular interactions, aiding in the rational design of novel therapeutics with improved potency and selectivity [36].

To determine the possible inhibition mechanism the tubulin protein was selected. The induced fit docking extra precision (XP) glide scores and MM-GBSA ΔG binding free energies of the *in vitro* most active compounds are given in Table 3.

The potential mechanism is highlighted by the exceptionally good docking scores and MM-GBSA ΔG free binding energies obtained against tubulin, suggesting that these molecules could be potential inhibitors tubulin. According to Table 3, compound **7** emerges as the best inhibitor candidate with docking score of −13.655 kcal/mol against tubulin. The docking scores of the other three compounds against tubulin range from −11.974 to −12.857 kcal/mol, indicating strong binding affinities.

These results indicate that the compounds have exceptionally high affinities for the tubulin protein, making them promising candidates for further development as tubulin inhibitors. According to the molecular docking results, the ligand-protein interactions of the four compounds given in Table 3 with tubulin were evaluated and analyzed separately in detail.

#### 2.3.1. Molecular docking interaction analysis on tubulin

Molecular docking 2D ligand-protein interactions (LPI) between the most active compounds and the active site of tubulin are given in Fig. 1. Fig. 1a represents the LPI between compound **5** and tubulin. As seen in Fig. 1a, the hydrazide carbonyl formed a hydrogen bond interaction with Ser-241. Moreover, the methoxy group of amid benzamide ring formed another hydrogen bond interaction with Cys-4. The anthranilic acid core formed two different π-π stacking interaction with Phe-202 and Phe-255. Finally, 2,4-dimethoxy benzylidene ring formed a π-cationic interaction (red line). Fig. 1b represents the LPI between compound **6** and tubulin. As seen in Fig. 1b, the oxygen atoms of both amide and hydrazide carbonyl formed two different hydrogen bond interactions with Asn-249 and Ser-241, respectively. The 3,4-dimethoxy benzylidene ring of compound **6** formed two different π-π stacking interaction with

**Table 3**
The IFD docking extra precision (XP) glide scores and MM-GBSA ΔG Binding free energies of most active compounds.

| PDB ID<br>Compounds | Induced Fit Docking XP Glide Scores (kcal/mol)<br>5FNV<br>Tubulin | MM-GBSA ΔG Binding Free Energies (kcal/mol)<br>5FNV<br>Tubulin |
|---|---|---|
| **5** | −11.974 | −84.84 |
| **6** | −12.362 | −87.63 |
| **7** | −13.655 | −86.79 |
| **11** | −12.857 | −71.07 |

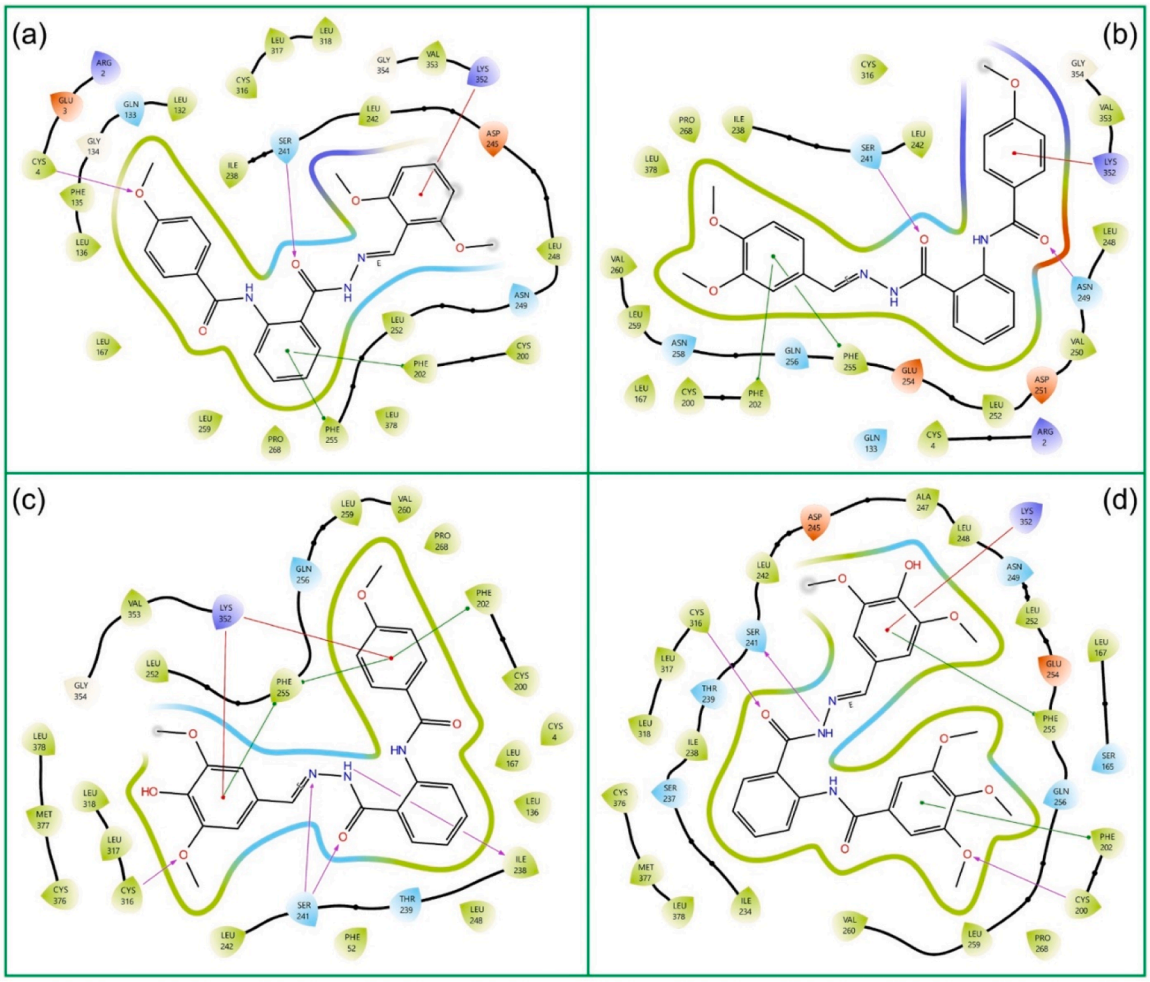


**Fig. 1.** Molecular docking 2D ligand-protein interactions between the most active compounds and the active site of tubulin. **(a)** Compound **5** and tubulin, **(b)** Compound **6** and tubulin, **(c)** Compound **7** and tubulin and **(d)** Compound **11** and tubulin.

Phe-202 and Phe-255. Finally, the benzamide ring formed a π-cationic interaction.

Fig. 1c depicts the LPI between compound **7** and tubulin. As seen in Fig. 1c, there are four hydrogen bond interactions between compound **7** and the active site of the tubulin. Ser-241 and Ile-238 formed three different hydrogen bond interaction with hydrazide moiety of compound **7**. Another hydrogen bond interaction was observed between methoxy group of benzylidene ring and Cys-316. Interestingly, Phe-255 and Lys-353 amino acid residues interacted with both the benzamide ring and the benzylidene ring of compound **7** at the same time and acted as a bridge between the two parts of the molecule. Both methoxylated rings had π-π stacking interactions with Phe-255 and π-cationic interactions with Lys-352. The benzamide ring also formed another π-π stacking interaction with Phe-202. These multiple interactions such as hydrogen bonds, π-π stacking interaction and π-cationic interactions clearly demonstrate that compound **7** has the best inhibition values and binding scores in both *in vitro* and *in silico* experiments. Finally, Fig. 1d shows the LPI between compound **11** and tubulin. As seen in Fig. 1d, while the hydrazide carbonyl formed a hydrogen bond interaction with Cys-316, the hydrazide nitrogen formed another hydrogen bond interaction with Ser-241. Moreover, there is an additional hydrogen bond interaction between Cys-200 and methoxy group of 3,4,5-trimethoxybenzamide ring. Benzamide and benzylidene rings formed a π-π stacking interaction with Phe-202 and Phe-255, respectively. The benzylidene ring also formed a π-cationic bond interaction with Lys-352.

Molecular docking 3D ligand-protein interactions between the most active compounds and the active site of tubulin are given in Fig. 2. In Fig. 2 the yellow dashes indicate the hydrogen bond interactions, red dashes represent the π-cationic bond interactions and the turquoise dashes indicate the π-π stacking interactions. Fig. 2a represents the 3D ligand protein interactions between tubulin and compounds **5.** As seen in Fig. 2a, while the hydrogen bond lengths with Ser-241 and Cys-4 were measured as 1.93 and 2.00 Å, respectively, the distances of Phe-202 and Phe-255 amino acids to the anthranilic acid moiety in π-π stacking interactions were measured as 4.36 and 5.33 Å. The distance of the π-cationic bond interaction between Lys-352 and the benzylidene ring is 4.77 Å. Fig. 2b represents the 3D ligand protein interactions between tubulin and compounds **6.** As seen in Fig. 2b, both carbonyl of compound **6** formed hydrogen bond interactions with 1.76 and 1.87 Å distances. The distances of hydrophobic interactions vary from 2.94 to 3.85 Å. Fig. 2c represents the 3D ligand protein interactions between tubulin and compounds **7.** It is clearly seen from Fig. 2c, compound **7**, the most potential inhibitor candidate in this series, exhibits multiple interactions with tubulin and that these interactions bind the molecule tightly to the active site of the enzyme. The interesting positions of Phe-202 and Lys-352 between the two benzene rings, along with the π-π stacking interactions and π-cationic interactions, significantly contribute to the stability of the ligand-protein complex. These interactions enhance the binding affinity, thereby increasing the potency of the inhibitory effect. In Fig. 2c, hydrogen bond lengths vary between 2.01 and 2.11 Å, and the distances of hydrophobic interactions vary between 3.92 and 5.24 Å.

As conclusion among the tested compounds, compound **7** exhibits

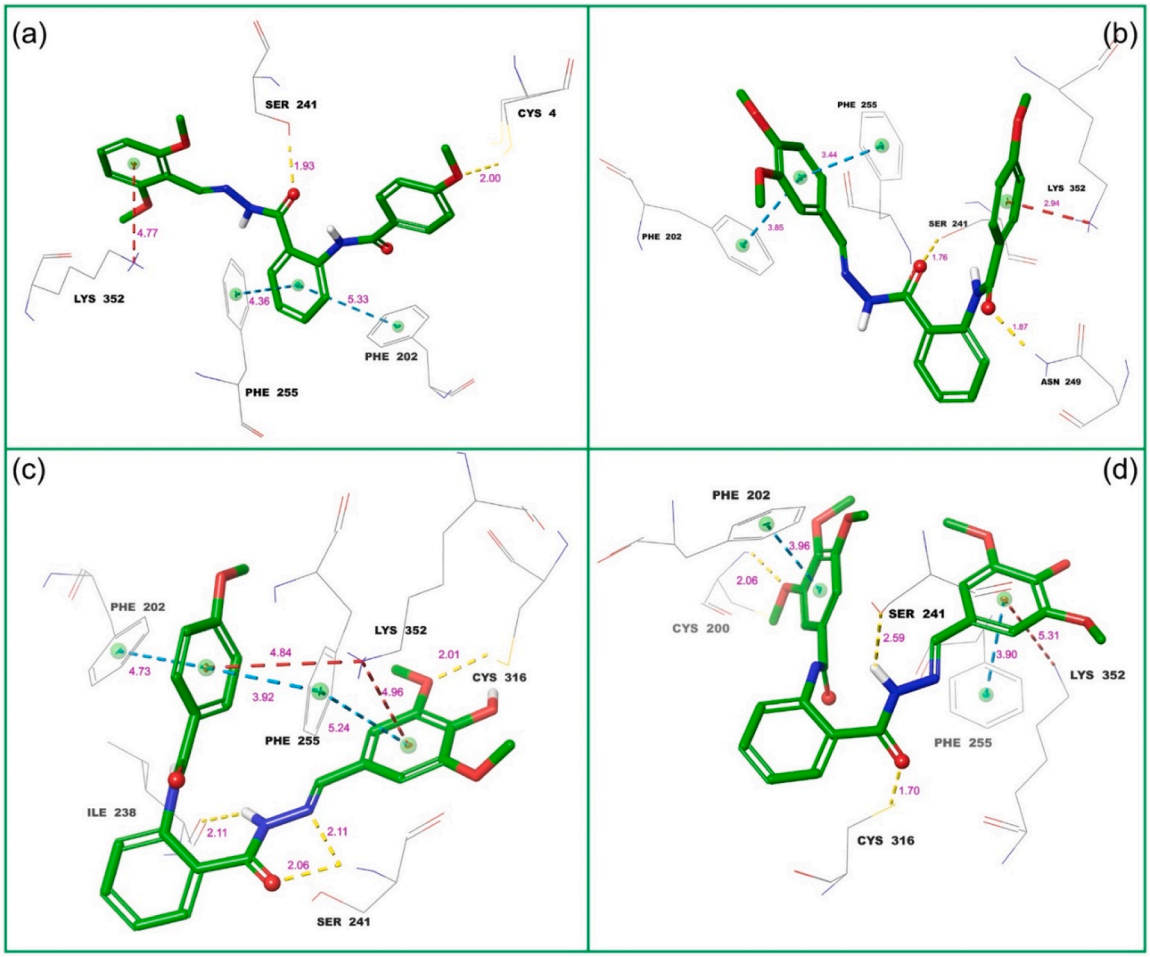


**Fig. 2.** Molecular docking 3D ligand-protein interactions between the most active compounds and the active site of tubulin. **(a)** Compound **5** and tubulin, **(b)** Compound **6** and tubulin, **(c)** Compound **7** and tubulin and **(d)** Compound **11** and tubulin.

the most extensive and diverse interactions with tubulin protein, highlighting its superior binding and inhibitory properties. Key interactions involve hydrogen bonds with Ser-241 and Ile-238, an additional hydrogen bond with Cys-316, and π-π stacking with Phe-202 and Phe-255. Compound **7** also engages in π-cationic interactions with Lys-352 and has its methoxylated rings involved in π-π stacking and π-cationic

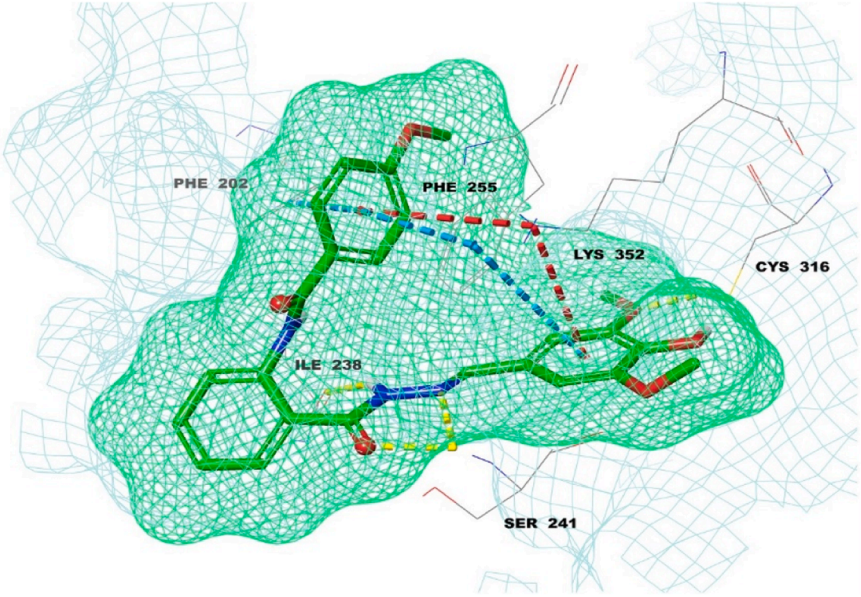


**Fig. 3.** The the ligand protein surface binding interaction of 7-tubulin.

interactions, with Phe-255 and Lys-353 bridging the benzamide and benzylidene rings. These robust interactions contribute to compound **7**′s exceptional binding affinity and inhibitory potency, making it the most effective among the tested compounds.

### 2.3.1. *Surface binding area analysis*

A surface binding area analysis was performed on the interactions of the most effective inhibitor candidate, compound **7**, with tubulin protein, to observe the ligand-protein fitting in the binding site. This analysis allows for a detailed observation of how well the ligand fits into the active site of the protein and maps the interactions within the protein backbone. The surface binding area analysis of the ligand-protein interactions for compound **7** with tubulin protein is presented in Fig. 3. In Fig. 3, while the turquoise mesh represents the surface binding area of protein, the green mesh represents the surface binding area of ligand. Compound **7** overlaps almost 95 % with the surface binding area of tubulin and is located in the binding site. However, the methoxy group 4-methoxybenzamide ring is relatively stay out of the surface binding

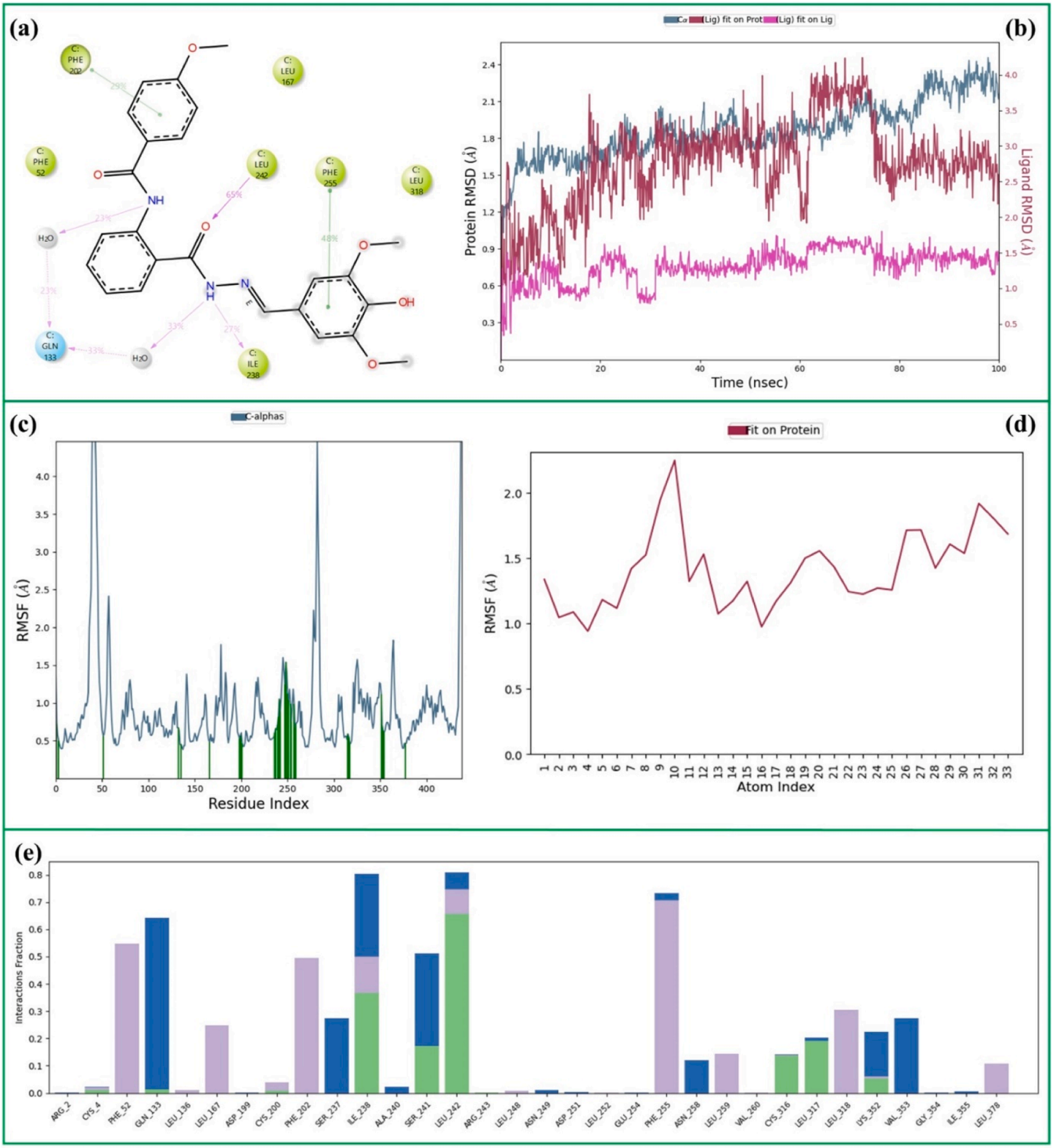


**Fig. 4.** The 100 ns MD simulation analysis of **7-tubulin** complex. (a) 2D key ligand protein interactions, (b) RMSD of ligand and protein, (c) RMSF of protein, (d) RMSF of ligand and (e) fractional interaction histogram.

area of the protein, but it is fixed in the binding site by hydrophobic interactions with Phe-255 near the binding site.

### 2.4. Molecular dynamics (MD) simulations

To evaluate the stabilities of the ligand protein complexes and determined the RMSD (root mean square deviation) and RMSF (root mean square fluctuation) of ligand and protein atoms, 100 ns MD simulation analysis of **7-tubulin** ligand protein complex was carried out. Due to the compound **7** is the most active and most selective compounds MD simulations were carried out using its complexes.

The MD simulation analysis of **7-tubulin** ligand protein complex is given in Fig. 4. Fig. 4a represents the 2D key ligand protein interactions during the simulation time with percentage values of **7-tubulin** complex. As seen in Fig. 4a, while the hydrazide carbonyl formed a hydrogen bond interaction with Leu-242 (65 % of the sim.) the hydrazide nitrogen formed another hydrogen bond interaction with Ile-238 (27 % of the sim.). Furthermore, both amide nitrogen and hydrazine nitrogen formed a water-bridged hydrogen bond interaction with Gln-133 during 23 % and 33 % of the simulation time, respectively. On the other hand, the benzylidene ring formed a π-π stacking interaction with Phe-255 (48 % of the sim.) and benzamide ring formed another π-π stacking interaction with Phe-202 (29 % of the sim.). The combination of hydrogen bonds and π-π stacking interactions ensures a stable and strong binding of the ligand to the protein.

Fig. 4b represents the RMSD of the ligand and protein Cα atoms of **7-tubulin** complex. In Fig. 4b, the average RMSD of protein Cα atoms was calculated as 2.0 Å (pale blue). The average RMSD of the ligand atoms was calculated as 2.5 Å (red). RMSD values of 2.0 Å for protein Cα atoms and 2.5 Å for ligand atoms indicate that the protein backbone and ligand atoms are mobile at an acceptable level. An average deviation of 1.25 Å from the initial position of the ligand (pink) caused the mobility of the ligand atoms, and this caused the RMSD value to increase in places. RMSD values of 2.0 Å for protein Cα atoms and 2.5 Å for ligand atoms indicate a moderate level of mobility for both the protein backbone and the ligand atoms, which is within an acceptable range for maintaining functional interactions. The average deviation of the ligand from its initial position was 1.25 Å (depicted in pink), contributing to the observed mobility of the ligand atoms and leading to partial increases in the RMSD value.

Figs. 4c and 4d represent the RMSF graphics of protein Cα atoms and ligand atoms of **7-tubulin** complex, respectively. The average RMSF values of protein Cα and ligand atoms were calculated as 1.1 Å and 1.5 Å respectively. Low fluctuations in both ligand and protein atoms indicate the stability of the ligand-protein complex, ensuring continuous and reliable binding. The slight increase in the RMSD value of the ligand atoms, due to their partial extension outside the binding area, is a minor deviation that does not significantly affect the stability of the complex. Instead, it highlights the ligand's flexibility in accommodating the binding surface area, contributing to a robust and adaptable interaction within the binding site.

Finally, Fig. 4e, shows the fractional interaction histogram of **7-tubulin** complex during the simulation time. The most abundant fractional interaction histograms were observed with Leu-242, Ile 238, Phe-255, Gln-133, Phe-52, Ser-241 and Phe-202, more than 50 % of the simulation time. These multiple amino acid interactions demonstrate that compound **7** can engage with the enzyme in a versatile manner.

In conclusion, the extensive molecular dynamics simulations of the **7-tubulin** ligand-protein complexes provide valuable insights into their stability and interactions. The analyses reveal strong hydrogen bond interactions between compound **7** and key amino acid residues, such as Leu-242, Ile-238, and Gln-133 in the **7-tubulin** complex. Additionally, π-π stacking interactions with residues such as Phe-255 and Phe-202 in the **7-tubulin** complex, further stabilize the ligand-protein interactions. The average RMSD of protein Cα atoms in the **7-tubulin** complex was calculated as 2.0 Å and the average RMSD of ligand atoms was calculated as 2.5 Å. Consequently, the **7-tubulin** complex demonstrates enhanced stability, likely attributed to the specific interactions and structural characteristics unique to the androgen receptor binding site.

### 2.5. ADME prediction

Comprehensive ADME (absorption, distribution, metabolism, and excretion) studies were conducted using *in silico* methods to assess the physicochemical descriptors, pharmacokinetic properties, and drug-likeness of the most active compounds. These studies involved predicting various parameters such as octanol/water partition coefficient, aqueous solubility, apparent Caco-2 cell permeability in nm/*sec*, brain/blood partition coefficient, apparent MDCK cell permeability in nm/*sec*, human oral absorption on a scale of 0–100 %, and the number of violations of Lipinski's rule of five and Jorgensen's rule of three parameters [37]. ADME prediction results of the most active compounds as well as reference drug doxorubicin are given in Table 4.

To qualify as a potential drug, molecules are typically assessed based on two key descriptors. The first is Lipinski's rule of five, which evaluates the number of violations against five specific criteria. The second is Jorgensen's rule of three, which assesses adherence to three distinct rules. Ideally, for a molecule to be considered a drug candidate, both descriptors should yield zero violations. However, it's acceptable for a molecule to violate up to three of Lipinski's five rules and up to two of Jorgensen's three rules [38,39].

According to the ADME analysis of compounds **5, 6, 7,** and **11,** along with the reference drug doxorubicin, molecular weight values range from 433.46 to 543.52 for the compounds, with compound **7** having the highest MW. The number of hydrogen bond donors *(dHB)* and acceptors *(aHB)* vary among the compounds, with compound **7** exhibiting the highest number of hydrogen bond acceptors. Predicted octanol/water partition coefficients *(QPlog Po/w)* range from 4.308 to 5.139, indicating favorable partitioning into lipophilic environments for all compounds. Aqueous solubility predictions *(QPlog S)* range from −6.182 to −5.855, with higher values indicating higher solubility. Compounds **5, 6,** and **7** demonstrate high apparent Caco-2 cell permeability *(QPPCaco)*, while compound **11** and doxorubicin show lower permeability. Predicted brain/blood partition coefficients (QPlog BB) suggest that compounds **5, 6,** and **7** may have better blood-brain barrier penetration compared to compound **11** and doxorubicin. Predicted apparent

**Table 4**
The ADME prediction of most active compounds and reference drug doxorubicin.

| Title* | 5 | 6 | 7 | 11 | Dox** |
|---|---|---|---|---|---|
| **MW** | 433.46 | 433.46 | 449.46 | 509.51 | 543.52 |
| **dHB** | 1 | 1 | 2 | 2 | 5 |
| **aHB** | 6 | 6 | 7 | 8 | 14 |
| **QPlog Po/w** | 5.139 | 4.997 | 4.308 | 4.354 | −0.52 |
| **QPlog S** | −6.471 | −6.368 | −6.182 | −5.855 | −2.28 |
| **QPlog BB** | −0.849 | −0.928 | −1.600 | −1.641 | −2.82 |
| **QPPCaco** | 1809 | 1535 | 485 | 509 | 3 |
| **QPPMDCK** | 939 | 786 | 226 | 238 | 1 |
| **%HOA** | 100 | 100 | 100 | 74 | 0 |
| **Ro5** | 1 | 0 | 0 | 2 | 3 |
| **Ro3** | 1 | 1 | 1 | 2 | 2 |

** Dox. = Doxorubicin,.

* **MW:** Molecular weight, 130–722; **dHB:** Number of hydrogen bond donors in an aqueous solution, 0.0 – 6.0; **aHB:** Number of hydrogen bond acceptors in an aqueous solution, 2.0 – 20.0; **QPlogPo/w:** Predicted octanol/water partition coefficient, –2.0 – 6.5; **QPlogS:** Predicted aqueous solubility, –6.5 – 0.5; **QPPCaco:** Predicted apparent Caco-2 cell permeability in nm/*sec*, <25 poor >500 great; **QPlogBB:** Predicted brain/blood partition coefficient, –3.0 – 1.2; **QPPMDCK:** Predicted apparent MDCK cell permeability in nm/*sec*, <25 poor >500 great;**%HOA:** Predicted human oral absorption on 0 to 100 % scale, >80 % is high <25 % is poor; **Ro5:** Number of violations of Lipinski's rule of five, max is 4; **Ro3:** Number of violations of Jorgensen's rule of three, max is 3.

MDCK cell permeability *(QPPMDCK)* values indicate good permeability for compounds **5, 6,** and **7.** Human oral absorption predictions *(%HOA)* suggest high oral absorption for compounds **5, 6,** and **7**, while compound 11 and Doxorubicin show lower absorption rates. Lipinski's rule of five *(Ro5)* violations are minimal for compounds **6, 7,** and **11**, but compound **5** has one violation. Jorgensen's rule of three *(Ro3)* violations are observed for compounds **5** and **11**, with one violation each, while compounds **6** and **7** have no violations. Overall, compounds **6** and **7** exhibit favorable ADME profiles with high permeability, solubility, and oral absorption, along with minimal violations of key drug-likeness rules.

### 2.6. Structure activity relationship

The structure-activity relationship (SAR) analysis reveals crucial insights into the impact of functional groups on the cytotoxic effects and molecular docking performance of the synthesized compounds. Compounds **5, 6, 7,** and **11**, exhibiting potent cytotoxicity and strong binding affinities against the tubulin protein, demonstrate distinct SAR patterns. According to the molecular docking results, the hydrazone moiety found in common in the compounds formed strong hydrogen with the amino acids found in the target receptors. The hydrazone moiety is necessary for the stabilization of ligand-protein interactions. However, the hydrazone moity is found in all molecules (Fig. 5). The type and position of substituents in the compounds are the main reason for the differences in activities.

Firstly, the presence of a *p*–$OCH_3$ group at A ring in compounds **5, 6, 7,** and **11** appears to enhance their cytotoxic effects against PC3 cells, as evidenced by their low $IC_{50}$ values. This substituent at $R_4$ likely contributes to improved molecular interactions with the target proteins, leading to enhanced potency. On the other hand, the methoxy groups located at positions 3, 4, and 5 of the C ring caused the activity to decrease. These groups probably created a steric hindrance, preventing the interaction of the ligand with the protein. The presence of an OH group at the para position of the C ring generally caused an increase in the cytotoxicity of the compounds. OH is known to be a group that easily forms hydrogen bonds and probably increased stability by forming strong hydrogen bonds with the tubulin protein. The cytotoxicity was reduced in compounds containing methoxy groups at the 3, 4, and 5 positions of the A ring due to steric effect compared to those containing methoxy groups at the 4 position. When the effects of ring B and its substituents on activity are examined, it is understood that they are not as effective as rings A and C. Overall, the SAR analysis underscores the importance of specific functional groups, particularly $OCH_3$ and OH, at specific positions in enhancing the cytotoxic effects and molecular interactions of the synthesized compounds. These findings provide valuable guidance for the rational design and optimization of novel anticancer agents targeting tubulin polimerization.

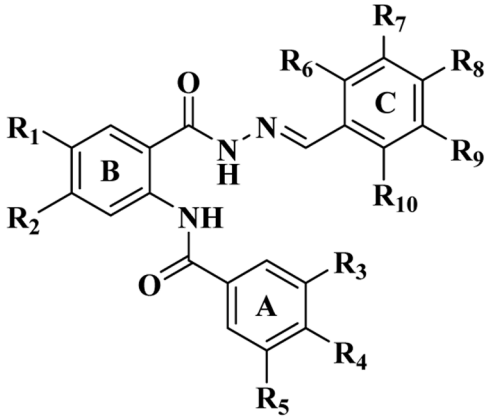


**Fig. 5.** The parts of the compounds **5–20**.

## 3. Conclusions

In this study, sixteen new polymethoxy-substituted hydrazone derivatives were synthesized and thoroughly characterized using FT-IR, $^1$H NMR, $^{13}$C NMR and HRMS spectroscopic techniques. The synthesized compounds were evaluated for their *in vitro* cytotoxic activity against human prostate cancer (PC3) and human umbilical vein endothelial (HUVEC) cell lines, using doxorubicin and temozolomide as reference inhibitors. Notably, compounds **5, 6, 7,** and **11** exhibited significant cytotoxic effects with high selectivity index, indicating their strong potential for targeting cancer cells preferentially over normal cells. Molecular docking studies and MM-GBSA binding free energy calculations were conducted to explore the binding affinities and potential inhibition mechanisms of these compounds against tubulin protein associated with prostate cancer growth. The results demonstrated that these compounds, particularly compound **7**, have strong binding affinities and favorable interaction profiles, highlighting their potential as effective anticancer agents.

Compound **7** stands out as a particularly promising candidate in this series of synthesized hydrazone derivatives. Its potency is underscored by an exceptionally low $IC_{50}$ value of 1.49 μM against PC3 cells, coupled with a remarkable selectivity index (SI) of 264.4. This high SI indicates a substantial ability to discriminate between cancerous and normal cells, a critical factor in the development of safer and more effective anticancer drugs. The cytotoxicity profile of compound **7** is superior to that of the reference drugs doxorubicin and temozolomide, not only in terms of potency but also in its selectivity for cancer cells.

Molecular docking studies revealed that compound **7** achieves impressive docking scores of −13.655 kcal/mol against tubulin protein. These scores are indicative of strong binding affinities. The MM-GBSA binding free energy calculations further support these findings, with compound **7** displaying a binding free energy of −86.79 kcal/mol against tubulin, showcasing its robust interaction with the target protein. Compound **7** formed critical hydrogen bonds with Ser-241 and Ile-238 in tubulin enhancing its binding stability. The methoxylated rings of compound **7** engage in π-π stacking and π-cationic interactions, particularly with Phe-255 and Lys-353 in tubulin further stabilizing the ligand-protein complex.

The ADME analysis of compound **7** showed high apparent Caco-2 and MDCK cell permeability, indicating good absorption potential. The predicted aqueous solubility (QPlog S) suggests that compound **7** has favorable solubility properties. Predictions for human oral absorption (%HOA) indicate high absorption rates. Finally, compound **7** showed minimal violations of Lipinski's rule of five (Ro5) and no violations of Jorgensen's rule of three (Ro3), suggesting good drug-likeness.

As a result, compound **7** is a leading candidate among the synthesized polymethoxy-substituted hydrazone derivatives due to its exceptional cytotoxicity, high selectivity index, strong binding affinities, and favorable ADME profile. Its ability to form stable and robust interactions with tubulin protein, along with its promising pharmacokinetic properties, positions it as a top candidate for further investigation and development as a novel candidate anticancer agent.

## 4. Material and methods

### 4.1. Chemistry

The chemicals used in the synthesis were purchased from Sigma Aldrich (Germany). Melting points were determined on WRS-2A Microprocessor Melting-point Apparatus and are uncorrected. The FTIR spectra of the compounds were recorded using ALPHA-P BRUKER FT-IR Spectrophotometer. $^1$H NMR and $^{13}$C NMR (APT) spectra were recorded on Bruker Avance NEO 500 and 125 MHz NMR spectrometer. Chemical shifts were reported as δ in ppm relative to tetramethyl silane (TMS) (δ 0.00 singlet) in deuterated dimethyl sulfoxide (DMSO-$d_6$). HRMS spectra were recorded by ESI technique on Thermo Fischer

Scientific Q Exactive™ Hybrid Triple Quadrupole-Orbitrap™. The spectra can be seen in the Supporting Information (SI) file.

*4.1.1. Synthesis of the target compounds (5–20)*

Methoxy substituted benzaldehyde (5 mmol) were added to a solution of the compounds **1–4** (5 mmol) in absolute ethanol (20 mL). Catalytic amounts (2–3 drops) of glacial acetic acid was added and the solution was refluxed for 2–3 h [40]. Reaction progress was monitored by TLC (Hex:EtOAc – 1:1). After completion, the solution was cooled to room temperature and formed solid was filtered off. The crude products were recrystallized from ethanol (Scheme 1).

*(E)-N-(2-(2-(2,6-Dimethoxybenzylidene)hydrazinecarbonyl)phenyl)−4-methoxybenzamide* ***(5)***

White solid, yield: 97 %, mp: 220–222 °C. FTIR ($cm^{-1}$): 3245, 3075, 1673, 1639, 1601. $^1$H NMR (500 MHz, DMSO) δ 12.12 (s, 1H), 11.92 (s, 1H), 8.81 (s, 1H), 8.58 (d, $J$ = 8.3 Hz, 1H), 7.93 (d, $J$ = 8.8 Hz, 3H), 7.62 (t, $J$ = 7.8 Hz, 1H), 7.41 (s, 1H), 7.25 (t, $J$ = 7.6 Hz, 1H), 7.14 (d, $J$ = 8.7 Hz, 2H), 7.09 – 7.03 (m, 2H), 3.85 (s, 3H), 3.83 (s, 3H), 3.78 (s, 3H). $^{13}$C NMR (125 MHz, DMSO) δ 165.4, 164.5, 162.7, 153.7, 153.0, 145.0, 140.2, 133.1, 129.5, 129.1, 127.0, 123.2, 123.1, 121.3, 120.4, 118.5, 114.7, 114.0, 109.7, 56.7, 56.0. HRMS: Chemical Formula: $C_{24}H_{23}N_3O_5$, calculated $[M\text{-}H]^+$ *m/z*: 432.1559, found $[M\text{-}H]^+$ *m/z*: 432.1569.

*(E)-N-(2-(2-(3,4-Dimethoxybenzylidene)hydrazinecarbonyl)phenyl)−4-methoxybenzamide* ***(6)***

White solid, yield: 98 %, mp: 230–232 °C. FTIR ($cm^{-1}$): 3204, 3080, 1671, 1632, 1596. $^1$H NMR (500 MHz, DMSO) δ 12.02 (s, 1H), 11.89 (s, 1H), 8.58 (d, $J$ = 8.3 Hz, 1H), 8.40 (s, 1H), 7.94 – 7.98 (m, 3H), 7.62 (t, $J$ = 7.8 Hz, 1H), 7.37 (s, 1H), 7.27 – 7.73 (m, 2H), 7.13 (d, $J$ = 8.8 Hz, 2H), 7.04 (d, $J$ = 8.3 Hz, 1H), 3.87 – 3.79 (m, 9H). $^{13}$C NMR (125 MHz, DMSO) δ 165.3, 164.5, 162.7, 151.5, 149.9, 149.6, 140.1, 133.0, 129.5, 129.0, 127.1, 127.0, 123.3, 122.8, 121.3, 120.7, 114.6, 111.9, 108.7, 55.9. HRMS: Chemical Formula: $C_{24}H_{23}N_3O_5$, calculated $[M\text{-}H]^+$ *m/z*: 432.1560, found $[M\text{-}H]^+$ *m/z*: 432.1563.

*(E)-N-(2-(2-(4-Hydroxy-3,5-dimethoxybenzylidene)hydrazinecarbonyl)phenyl)−4-methoxybenzamide* ***(7)***

White solid, yield: 97 %, mp: 231–233 °C. FTIR ($cm^{-1}$): 3423, 3215, 3060, 1661, 1644, 1600. $^1$H NMR (500 MHz, DMSO) δ 12.00 (s, 1H), 11.87 (s, 1H), 9.00 (s, 1H), 8.57 (d, $J$ = 8.3 Hz, 1H), 8.35 (s, 1H), 7.93 (d, $J$ = 8.8 Hz, 2H), 7.89 (d, $J$ = 7.4 Hz, 1H), 7.62 (t, $J$ = 7.8 Hz, 1H), 7.26 (t, $J$ = 7.4 Hz, 1H), 7.13 (d, $J$ = 8.8 Hz, 2H), 7.02 (s, 2H), 3.84 (s, 9H). $^{13}$C NMR (125 MHz, DMSO) δ 165.3, 164.5, 162.7, 150.3, 148.6, 140.0, 138.8, 132.9, 129.5, 129.0, 127.0, 124.7, 123.3, 121.3, 120.8, 114.6, 105.3, 56.5, 55.9. HRMS: Chemical Formula: $C_{24}H_{23}N_3O_6$, calculated $[M\text{-}H]^+$ *m/z*: 448.1507, found $[M\text{-}H]^+$ *m/z*: 448.1515.

*(E)-N-(2-(2-(3,4,5-Trimethoxybenzylidene)hydrazinecarbonyl)phenyl)−4-methoxybenzamide* ***(8)***

White solid, yield: 98 %, mp: 234–236 °C. FTIR ($cm^{-1}$): 3209, 3059, 1662, 1646, 1600. $^1$H NMR (500 MHz, DMSO) δ 12.11 (s, 1H), 11.79 (s, 1H), 8.55 (d, $J$ = 8.3 Hz, 1H), 8.39 (s, 1H), 7.94 – 7.88 (m, 3H), 7.62 (t, $J$ = 7.8 Hz, 1H), 7.27 (t, $J$ = 7.6 Hz, 1H), 7.12 (d, $J$ = 8.5 Hz, 2H), 7.05 (s, 2H), 3.85 (s, 9H), 3.72 (s, 3H). $^{13}$C NMR (125 MHz, DMSO) δ 165.4, 164.6, 162.7, 153.7, 149.6, 140.0, 139.9, 133.0, 130.0, 129.5, 129.1, 127.0, 123.3, 121.5, 120.9, 114.6, 105.0, 60.6, 56.4, 55.9. HRMS: Chemical Formula: $C_{25}H_{25}N_3O_6$, calculated $[M\text{-}H\text{+}Na]^+$ *m/z*: 485.2763, found $[M\text{-}H\text{+}Na]^+$ *m/z*: 485.2793.

*(E)-N-(2-(2-(2,6-Dimethoxybenzylidene)hydrazinecarbonyl)phenyl)−3,4,5-trimethoxybenzamide* ***(9)***

White solid, yield: 95 %, mp: 157–159 °C. FTIR ($cm^{-1}$): 3222, 3069, 1639, 1601. $^1$H NMR (500 MHz, DMSO) δ 12.08 (s, 1H), 11.69 (s, 1H), 8.80 (s, 1H), 8.38 (d, $J$ = 8.2 Hz, 1H), 7.90 (d, $J$ = 7.7 Hz, 1H), 7.62 (t, $J$ = 7.8 Hz, 1H), 7.39 (s, 1H), 7.30 – 7.24 (m, 3H), 7.08 – 7.01 (m, 2H), 3.89 (s, 6H), 3.81 (s, 3H), 3.76 (s, 6H). $^{13}$C NMR (125 MHz, DMSO) δ 165.1, 164.8, 153.7, 153.4, 152.9, 144.6, 141.1, 139.4, 132.8, 130.4, 129.1, 123.8, 123.1, 122.2, 122.0, 118.4, 113.9, 109.66, 105.2, 60.6, 56.5, 55.8. HRMS: Chemical Formula: $C_{26}H_{27}N_3O_7$, calculated $[M\text{-}H]^+$ *m/z*: 494.1927, found $[M\text{-}H]^+$ *m/z*: 494.1910.

*(E)-N-(2-(2-(3,4-Dimethoxybenzylidene)hydrazinecarbonyl)phenyl)−3,4,5-trimethoxybenzamide* ***(10)***

White solid, yield: 97 %, mp: 190–192 °C. FTIR ($cm^{-1}$): 3221, 3083, 1683, 1634, 1586. $^1$H NMR (500 MHz, DMSO) δ 11.98 (s, 1H), 11.65 (s, 1H), 8.37 (s, 1H), 7.86 (d, $J$ = 7.6 Hz, 1H), 7.62 (t, $J$ = 7.8 Hz, 1H), 7.35 (s, 1H), 7.31 – 7.24 (m, 3H), 7.20 (d, $J$ = 8.3 Hz, 1H), 7.03 (d, $J$ = 8.3 Hz, 1H), 3.89 (s, 6H), 3.82 (s, 3H), 3.81 (s, 3H), 3.75 (s, 3H). $^{13}$C NMR (125 MHz, DMSO) δ 165.1, 164.8, 153.4, 151.4, 149.5, 149.4, 141.1, 139.3, 132.7, 130.4, 129.0, 127.2, 123.8, 122.6, 122.5, 122.1, 111.9, 108.6, 105.3, 60.6, 56.5, 56.0. HRMS: Chemical Formula: $C_{26}H_{27}N_3O_7$, calculated $[M\text{+}Na]^+$ *m/z*: 516.1747, found $[M + N]^+$ *m/z*: 516.1754.

*(E)-N-(2-(2-(4-Hydroxy-3,5-dimethoxybenzylidene)hydrazinecarbonyl)phenyl)−3,4,5-trimethoxybenzamide* ***(11)***

White solid, yield: 95 %, mp: 222–224 °C. FTIR ($cm^{-1}$): 3271, 3063, 1653, 1582. $^1$H NMR (500 MHz, DMSO) δ 11.97 (s, 1H), 11.63 (s, 1H), 8.97 (s, 1H), 8.48 – 8.19 (m, 2H), 7.85 (d, $J$ = 7.6 Hz, 1H), 7.62 (t, $J$ = 7.8 Hz, 1H), 7.31 – 7.24 (m, 3H), 6.99 (s, 2H), 3.89 (s, 6H), 3.83 (s, 6H), 3.75 (s, 3H). $^{13}$C NMR (125 MHz, DMSO) δ 165.0, 164.9, 153.4, 149.8, 148.6, 141.1, 139.2, 138.6, 132.6, 130.5, 129.0, 124.8, 123.9, 122.7, 122.2, 105.3, 105.2, 60.6, 56.5. HRMS: Chemical Formula: $C_{26}H_{27}N_3O_8$, calculated $[M + H]^+$ *m/z*: 510.1876, found $[M + H]^+$ *m/z*: 510.1868.

*(E)-N-(2-(2-(3,4,5-Trimethoxybenzylidene)hydrazinecarbonyl)phenyl)−3,4,5-trimethoxybenzamide* ***(12)***

White solid, yield: 97 %, mp: 246–248 °C. FTIR ($cm^{-1}$): 3207, 3066, 1651, 1602. $^1$H NMR (500 MHz, DMSO) δ 12.07 (s, 1H), 11.59 (s, 1H), 8.37 (s, 1H), 8.34 (d, $J$ = 7.5 Hz, 1H), 7.86 (d, $J$ = 7.4 Hz, 1H), 7.63 (t, $J$ = 7.5 Hz, 1H), 7.30 (t, $J$ = 7.4 Hz, 1H), 7.26 (s, 2H), 7.03 (s, 2H), 3.89 (s, 6H), 3.85 (s, 6H), 3.76 (s, 3H), 3.72 (s, 3H). $^{13}$C NMR (125 MHz, DMSO) δ 164.7, 164.4, 153.2, 152.9, 148.7, 140.8, 139.5, 138.8, 132.2, 129.9, 129.6, 128.6, 123.4, 122.1, 121.7, 104.9, 104.5, 60.1, 56.1. HRMS: Chemical Formula: $C_{27}H_{29}N_3O_8$, calculated $[M\text{-}H]^+$ *m/z*: 522.1876, found $[M\text{-}H]^+$ *m/z*: 522.1882.

*(E)-N-(2-(2-(2,6-Dimethoxybenzylidene)hydrazinecarbonyl)−4,5-dimethoxyphenyl)−4-methoxybenzamide* ***(13)***

White solid, yield: 97 %, mp: 247–249 °C. FTIR ($cm^{-1}$): 3227, 3073, 1637, 1604. $^1$H NMR (500 MHz, DMSO) δ 12.42 (s, 1H), 11.91 (s, 1H), 8.81 (s, 1H), 8.46 (s, 1H), 7.93 (d, $J$ = 8.6 Hz, 2H), 7.50 (s, 1H), 7.42 (s, 1H), 7.13 (d, $J$ = 8.6 Hz, 2H), 7.08 – 7.02 (m, 2H), 3.88 – 3.83 (m, 12H), 3.78 (s, 3H). $^{13}$C NMR (125 MHz, DMSO) δ 165.3, 164.3, 162.6, 153.7, 152.9, 152.5, 144.3, 144.0, 136.3, 129.3, 127.1, 123.1, 118.3, 114.6, 113.8, 111.9, 110.5, 109.8, 104.5, 56.6, 56.0. HRMS: Chemical Formula: $C_{26}H_{27}N_3O_7$, calculated $[M\text{-}H]^+$ *m/z*: 492.1771, found $[M\text{-}H]^+$ *m/z*: 492.1788.

*(E)-N-(2-(2-(3,4-Dimethoxybenzylidene)hydrazinecarbonyl)−4,5-dimethoxyphenyl)−4-methoxybenzamide* ***(14)***

White solid, yield: 96 %, mp: 219–221 °C. FTIR ($cm^{-1}$): 3169, 3056, 1673, 1622, 1598. $^1$H NMR (500 MHz, DMSO) δ 12.36 (s, 1H), 11.81 (s, 1H), 8.45 (s, 1H), 8.41 (s, 1H), 7.93 (d, $J$ = 8.6 Hz, 2H), 7.47 (s, 1H), 7.37 (s, 1H), 7.23 (d, $J$ = 8.1 Hz, 1H), 7.11 (d, $J$ = 8.6 Hz, 2H), 7.03 (d, $J$ = 8.3 Hz, 1H), 3.90 – 3.79 (m, 15H). $^{13}$C NMR (125 MHz, DMSO) δ 165.3, 164.3, 162.6, 152.4, 151.4, 149.6, 149.6, 144.0, 136.2, 129.3, 127.2, 127.1, 122.7, 114.6, 112.0, 111.9, 110.9, 108.7, 104.6, 56.5, 55.9. HRMS: Chemical Formula: $C_{26}H_{27}N_3O_7$, calculated $[M\text{-}H]^+$ *m/z*: 492.1771, found $[M\text{-}H]^+$ *m/z*: 492.1777.

*(E)-N-(2-(2-(4-Hydroxy-3,5-dimethoxybenzylidene)hydrazinecarbonyl)−4,5-dimethoxyphenyl)−4-methoxybenzamide* ***(15)***

White solid, yield: 96 %, mp: 249–251 °C. FTIR ($cm^{-1}$): 3380, 3227, 3078, 1635, 1607. $^1$H NMR (500 MHz, DMSO) δ 12.32 (s, 1H), 11.79 (s, 1H), 9.00 (s, 1H), 8.43 (s, 1H), 8.37 (s, 1H), 7.93 (d, $J$ = 8.6 Hz, 2H), 7.46 (s, 1H), 7.12 (d, $J$ = 8.6 Hz, 2H), 7.02 (s, 2H), 3.87 – 3.84 (m, 15H). $^{13}$C NMR (125 MHz, DMSO) δ 165.2, 164.3, 162.6, 152.4, 150.1, 148.6, 144.0, 138.7, 136.0, 129.3, 127.1, 124.7, 114.6, 112.1, 111.1, 105.3, 104.6, 56.5, 55.9. HRMS: Chemical Formula: $C_{26}H_{27}N_3O_8$, calculated $[M\text{+}Na]^+$ *m/z*: 532.1496, found $[M\text{+}Na]^+$ *m/z*: 532.1483.

*(E)-N-(2-(2-(3,4,5-Trimethoxybenzylidene)hydrazinecarbonyl)−4,5-dimethoxyphenyl)−4-methoxybenzamide* ***(16)***

White solid, yield: 95 %, mp: 235–237 °C. FTIR ($cm^{-1}$): 3182, 3052, 1670, 1628, 1597. $^{1}H$ NMR (500 MHz, DMSO) δ 12.24 (s, 1H), 11.89 (s, 1H), 8.41 (d, $J = 4.9$ Hz, 2H), 7.93 (d, $J = 8.6$ Hz, 2H), 7.46 (s, 1H), 7.13 (d, $J = 8.6$ Hz, 2H), 7.05 (s, 2H), 3.87 – 3.84 (m, 15H), 3.72 (s, 3H). $^{13}C$ NMR (125 MHz, DMSO) δ 165.3, 164.3, 162.7, 153.7, 152.4, 149.4, 144.1, 139.9, 136.0, 130.0, 129.3, 127.1, 114.6, 112.1, 111.1, 104.9, 104.7, 60.6, 56.4, 55.9. HRMS: Chemical Formula: $C_{27}H_{29}N_3O_8$, calculated $[M-H]^+$ *m/z*: 522.1876, found $[M-H]^+$ *m/z*: 522.1882.

*(E)-N-(2-(2-(2,6-Dimethoxybenzylidene)hydrazinecarbonyl)−4,5-dimethoxyphenyl)−3,4,5-trimethoxybenzamide* ***(17)***

White solid, yield: 94 %, mp: 208–210 °C. FTIR ($cm^{-1}$): 3250, 1657, 1632, 1608. $^{1}H$ NMR (500 MHz, DMSO) δ 12.26 (s, 1H), 11.88 (s, 1H), 8.80 (s, 1H), 8.29 (s, 1H), 7.48 (s, 1H), 7.40 (d, $J = 2.7$ Hz, 1H), 7.26 (s, 2H), 7.07 – 7.00 (m, 2H), 3.90 – 3.75 (m, 21H). $^{13}C$ NMR (125 MHz, DMSO) δ 165.1, 164.5, 153.7, 153.4, 152.8, 152.3, 144.4, 144.1, 141.1 135.5, 130.5, 123.2, 118.3, 113.8, 111.8, 111.8, 109.6, 105.1, 105.0, 60.6, 56.5, 56.0. HRMS: Chemical Formula: $C_{28}H_{31}N_3O_9$, calculated $[M-H]^+$ *m/z*: 552.1982, found $[M-H]^+$ *m/z*: 552.2010.

*(E)-N-(2-(2-(3,4-Dimethoxybenzylidene)hydrazinecarbonyl)−4,5-dimethoxyphenyl)−3,4,5-trimethoxybenzamide* ***(18)***

White solid, yield: 96 %, mp: 204–206 °C. FTIR ($cm^{-1}$): 3189, 3067, 1668, 1626, 1595. $^{1}H$ NMR (500 MHz, DMSO) δ 12.15 (s, 1H), 11.78 (s, 1H), 8.40 (s, 1H), 8.25 (s, 1H), 7.44 (s, 1H), 7.36 (s, 1H), 7.26 (s, 2H), 7.21 (d, $J = 8.1$ Hz, 1H), 7.03 (d, $J = 8.3$ Hz, 1H), 3.90 – 3.75 (m, 21H). $^{13}C$ NMR (125 MHz, DMSO) δ 165.0, 164.5, 153.4, 152.2, 151.4, 149.5, 149.3, 144.4, 141.1, 135.2, 130.5, 127.3, 122.5, 112.4, 111.9, 108.7, 105.2, 105.1, 60.6, 56.5, 56.0. HRMS: Chemical Formula: $C_{28}H_{31}N_3O_9$, calculated $[M-H]^+$ *m/z*: 552.1982, found $[M-H]^+$ *m/z*: 552.1987.

*(E)-N-(2-(2-(4-Hydroxy-3,5-dimethoxybenzylidene) hydrazinecarbonyl)−4,5-dimethoxyphenyl)−3,4,5-trimethoxybenzamide* ***(19)***

White solid, yield: 95 %, mp: 228–230 °C. FTIR ($cm^{-1}$): 3382, 3223, 1659, 1637, 1605. $^{1}H$ NMR (500 MHz, DMSO) δ 12.15 (s, 1H), 11.78 (s, 1H), 8.97 (s, 1H), 8.35 (s, 1H), 8.23 (s, 2H), 7.44 (s, 1H), 7.26 (s, 2H), 7.00 (s, 2H), 3.89 – 3.75 (m, 21H). $^{13}C$ NMR (125 MHz, DMSO) δ 165.0, 164.5, 153.4, 152.1, 149.8, 148.6, 144.4, 141.1, 138.6, 135.1, 130.5, 124.8, 112.5, 111.9, 105.2, 105.1, 60.6, 56.4, 56.0. HRMS: Chemical Formula: $C_{28}H_{31}N_3O_{10}$, calculated $[M-H]^+$ *m/z*: 568.1931, found $[M-H]^+$ *m/z*: 568.1946.

*(E)-N-(2-(2-(3,4,5-Trimethoxybenzylidene)hydrazinecarbonyl)−4,5-dimethoxyphenyl)−3,4,5-trimethoxybenzamide* ***(20)***

White solid, yield: 96 %, mp: 222–224 °C. FTIR ($cm^{-1}$): 3204, 1658, 1630, 1610. $^{1}H$ NMR (500 MHz, DMSO) δ 12.08 (s, 1H), 11.88 (s, 1H), 8.39 (s, 1H), 8.21 (s, 1H), 7.44 (s, 1H), 7.26 (s, 2H), 7.03 (s, 2H), 3.89 – 3.71 (m, 24H). $^{13}C$ NMR (125 MHz, DMSO) δ 165.1, 164.6, 153.7, 153.4, 152.2, 149.0, 144.5, 141.1, 139.8, 135.1, 130.5, 130.1, 112.5, 112.0, 105.3, 105.1, 104.8, 60.6, 56.5, 56.0. HRMS: Chemical Formula: $C_{29}H_{33}N_3O_{10}$, calculated $[M-H]^+$ *m/z*: 582.2088, found $[M-H]^+$ *m/z*: 582.2092.

### 4.2. Biological activity studies

#### 4.2.1. Cell culture

Human prostate adenocarcinoma cells (PC3) and Human Umbilical Vein Endothelial Cells (HUVEC) were cultured in DMEM-F12 medium (Gibco, MD, USA) supplemented with 10 % fetal bovine serum (FBS) (Gibco, MD, USA) and 1 % penicillin/streptomycin under 5 % $CO_2$ in a humidified atmosphere. Compounds were tested on HUVEC as normal cells to check their non-toxic activity and PC3 cells to consider effect on tumor cells.

#### 4.2.2. Cell viability assay

The effects of compounds on cell viability against PC3 and HUVEC cells were evaluated using 3-(4,5-dimethylthiazol-2-yl)−2,5-diphenyltetrazolium bromide (MTT)) proliferation assay. PC3 and HUVEC cells were seeded in 96-well plates ($1 \times 10^4$ cells/per well) and after overnight, treated with eight different concentrations of compounds (1, 3.125, 6.25, 12.5, 25, 50, 100 and 200 μM) for 24 h. After treatment, MTT (final concentration 0.1 mg/mL) was added, and cell were incubated for 4 h at 37 °C. Following the aspiration of supernatants, DMSO was added, and the mixture was further incubated at room temperature in the dark for 30 min. Absorbance was measured at 570 nm using a microplate reader (BioTek Instruments, Inc, USA). Selectivity of compounds on cancer cells can be expressed by the selectivity index (SI) value, which was determined using the following formula:

Selectivity index (SI)=$IC_{50}$ normal cells/ $IC_{50}$ cancerous cells [41].

#### 4.2.3. Statistical anaylis

The data was expressed as a mean ± standard error of the mean (SEM) with each experiment consisting of triplicates. Statistical differences between untreated cells and treated cells were determined using Student's *t*-test. Multiple comparisons between the treatment groups were performed using ANOVA followed by Tukey's post-hoc test by GraphPad Prism 6.01 [41].

### 4.3. Computational studies

Molecular Docking studies using carried out by Schrödinger Molecular Modelling Software (2024–1) with Maestro (13.9) interface. MD simulations were carried out using Desmond (D. E. Shaw Research) with Maestro (13.5) interface.

#### 4.3.1. Preparation ligands and proteins

The known methods that previously published by our research group were used to perform protein and ligand preparation [42]. The 3D X-ray crystallographic structures of the target proteins were obtained from the Protein Data Bank, accessible via the RCSB website (https://www.rcsb.org). In this study, androgen receptor (AR) (PDB ID: 2PNU), tubulin (PDB ID: 5FNV), mTOR (PDB ID: 4JT5), PARP1 (PDB ID: 5WS1), and PI3K (PDB ID: 4L23) were used to carried out for all *in silico* studies. Careful preparation and refinement of these protein structure was carried out using the Protein Preparation Wizard module within Schrödinger Maestro 13.9.

#### 4.3.2. Glide docking and induced fit docking

The known methods that previously published by our research group were used to perform glide docking and induced fit docking [43].

#### 4.3.3. Prime MM-GBSA analysis

The known methods that previously published by our research group were used to perform prime MM-GBSA analysis [41].

#### 4.3.4. Molecular dynamics simulations

The known methods that previously published by our research group were used to perform molecular dynamics simulations [41].

#### 4.3.5. ADME prediction

The known methods that previously published by our research group were used to perform *in silico* ADME Prediction [41].

## CRediT authorship contribution statement

**Feyzi Sinan Tokalı:** Investigation, Validation, Writing – original draft. **Halil Şenol:** Investigation, Validation, Writing – original draft. **Şeyma Ateşoğlu:** Investigation, Writing – review & editing. **Pelin Tokalı:** Investigation, Writing – review & editing. **Fahri Akbaş:** Investigation, Writing – review & editing.

## Declaration of competing interest

The authors declare that they have no known competing financial interests or personal relationships that could have appeared to influence

the work reported in this paper.

## Data availability

Data will be made available on request.

## Supplementary materials

Supplementary material associated with this article can be found, in the online version, at doi:10.1016/j.molstruc.2024.139519.

## References


[1] D.M. Hausman, What is cancer? Perspect. Biol. Med. 62 (2019) 778–784, https://doi.org/10.1353/pbm.2019.0046.

[2] S. Hirabayashi, Y. Li, N. Ohta, A. Ishibashi, Y. Yoshikawa, B. Lin, M. Fumimoto, T. Takehara, K. Nunomura, T. Suzuki, J. Haruta, K. Nimura, M. Arisawa, Design and synthesis of ether derivatives of spliceostatin A and their biological evaluation towards prostate cancer treatment, Tetrahedron Lett 114 (2023) 154288, https://doi.org/10.1016/j.tetlet.2022.154288.

[3] A.A. Shafi, A.E. Yen, N.L. Weigel, Androgen receptors in hormone-dependent and castration-resistant prostate cancer, Pharmacol. Ther. 140 (2013) 223–238, https://doi.org/10.1016/j.pharmthera.2013.07.003.

[4] R.B. Marques, N.F. Dits, S. Erkens-Schulze, W.M. van Weerden, G. Jenster, Bypass mechanisms of the androgen receptor pathway in therapy-resistant prostate cancer cell models, PLoS ONE 5 (2010) e13500, https://doi.org/10.1371/journal.pone.0013500.

[5] D. Poirier, R. Maltais, J.A. Rousseau, J. Roy, S. Phoenix, F. Cortés-Benítez, R. Lecomte, Chemical synthesis of fluorinated and iodinated 17β-HSD3 inhibitors and evaluation for imaging prostate cancer tumors and tissue biodistribution, Bioorg. Chem. 129 (2022) 106145, https://doi.org/10.1016/j.bioorg.2022.106145.

[6] H. Sung, J. Ferlay, R.L. Siegel, M. Laversanne, I. Soerjomataram, A. Jemal, F. Bray, Global cancer statistics 2020: GLOBOCAN estimates of incidence and mortality worldwide for 36 cancers in 185 countries, CA Cancer J. Clin. 71 (2021) 209–249, https://doi.org/10.3322/caac.21660.

[7] M. Lopus, Tubulin-targeted cancer chemotherapeutics: advances and challenges, Cur. Top. Med. Chem. 17 (2017), https://doi.org/10.2174/1568026617221707261136l4, 2522-2522.

[8] M. Lopus, Advances in tubulin-targeted cancer chemotherapeutics, Int. J. Mol. Med. 36 (2015), https://doi.org/10.2174/1568026617221707261136l4. S8-S8.

[9] M. Jumaah, T.D. Wahyuningsih, M. Khairuddean, 3,4,5-Trimethoxychalcones tubulin inhibitors with a stable colchicine binding site as potential anticancer agents, Indones. J. Chem. 22 (2022) 72790, https://doi.org/10.22146/ijc.72790.

[10] T. Constantinescu, A.G. Mihis, Two important anticancer mechanisms of natural and synthetic chalcones, Int. J. Mol. Sci. 23 (2022), https://doi.org/10.3390/ijms231911595.

[11] C. Wang, J. Chang, S. Yang, L. Shi, Y. Zhang, W. Liu, J. Meng, J. Zeng, R. Zhang, D. Xing, Advances in antitumor research of CA-4 analogs carrying quinoline scaffold, Front. Chem. 10 (2022) 1040333, https://doi.org/10.3389/fchem.2022.1040333.

[12] M.A. Mohamed, R.R. Ayyad, T.Z. Shawer, A.A. Abdel-Aziz, A.S. El-Azab, Synthesis and antitumor evaluation of trimethoxyanilides based on 4(3H)-quinazolinone scaffolds, Eur. J. Med. Chem. 112 (2016) 106–113, https://doi.org/10.1016/j.ejmech.2016.02.002.

[13] R. Patil, S.A. Patil, K.D. Beaman, S.A. Patil, Indole molecules as inhibitors of tubulin polymerization: potential new anticancer agents, an update (2013-2015), Future Med. Chem. 8 (2016) 1291–1316, https://doi.org/10.4155/fmc-2016-0047.

[14] T.A. Yousef, A.G. Alhamzani, M.M. Abou-Krisha, G. Kanthimathi, M.S. Raghu, K. Y. Kumar, M.K. Prashanth, B.H. Jeon, Synthesis, molecular docking study and anticancer activity of novel 1,3,4-oxadiazole derivatives as potential tubulin inhibitors, Heliyon 9 (2023) e13460, https://doi.org/10.1016/j.heliyon.2023.e13460.

[15] N. Mur Blanch, G.G. Chabot, L. Quentin, D. Scherman, S. Bourg, D. Dauzonne, *In vitro* and *in vivo* biological evaluation of new 4,5-disubstituted 1,2,3-triazoles as cis-constrained analogs of combretastatin A4, Eur. J. Med. Chem. 54 (2012) 22–32, https://doi.org/10.1016/j.ejmech.2012.04.017.

[16] Y.P. Quan, L.P. Cheng, T.C. Wang, W. Pang, F.H. Wu, J.W. Huang, Molecular modeling study, synthesis and biological evaluation of combretastatin A-4 analogues as anticancer agents and tubulin inhibitors, Med. Chem. Comm. 9 (2018) 316–327, https://doi.org/10.1039/C7MD00416H.

[17] A.M. Shawky, N.A. Ibrahim, A.N. Abdalla, M.A.S. Abourehab, A.M. Gouda, Novel pyrrolizines bearing 3,4,5-trimethoxyphenyl moiety: design, synthesis, molecular docking, and biological evaluation as potential multi-target cytotoxic agents, J. Enzyme Inhib. Med. Chem. 36 (2021) 1313–1333, https://doi.org/10.1080/14756366.2021.1937618.

[18] C.Y. Lee, C.N. Nanah, R.A. Held, A.R. Clark, U.G. Huynh, M.C. Maraskine, R. L. Uzarski, J. McCracken, A. Sharma, Effect of electron donating groups on polyphenol-based antioxidant dendrimers, Biochimie 111 (2015) 125–134, https://doi.org/10.1016/j.biochi.2015.02.001.

[19] H. Yang, Z. Du, W. Wang, M. Song, K. Sanidad, E. Sukamtoh, J. Zheng, L. Tian, H. Xiao, Z. Liu, G. Zhang, Structure-Activity Relationship of Curcumin: role of the Methoxy Group in Anti-inflammatory and Anticolitis Effects of Curcumin, J. Agric. Food Chem. 65 (2017) 4509–4515, https://doi.org/10.1021/acs.jafc.7b01792.

[20] W. Gładkowski, M. Siepka, T. Janeczko, E. Kostrzewa-Susłow, J. Popłoński, M. Mazur, B. Żarowska, W. Łaba, G. Maciejewska, C. Wawrzeńczyk, Synthesis and antimicrobial activity of methoxy- substituted γ-Oxa-ε-lactones derived from flavanones, Molecules 24 (2019) 24224151, https://doi.org/10.3390/molecules24224151.

[21] M. Ma, L. Sun, H. Lou, M. Ji, Synthesis and biological evaluation of Combretastatin A-4 derivatives containing a 3′-O-substituted carbonic ether moiety as potential antitumor agents, Chem. Cent. J. 7 (2013) 179, https://doi.org/10.1186/1752-153X-7-179.

[22] M.N. Semenova, D.V. Demchuk, D.V. Tsyganov, N.B. Chernysheva, A.V. Samet, E. A. Silyanova, V.P. Kislyi, A.S. Maksimenko, A.E. Varakutin, L.D. Konyushkin, M. M. Raihstat, A.S. Kiselyov, V.V. Semenov, Sea urchin embryo model as a reliable in vivo phenotypic screen to characterize selective antimitotic molecules. Comparative evaluation of combretapyrazoles, -isoxazoles, -1,2,3-triazoles, and -pyrroles as tubulin-binding agents, ACS Comb. Sci. 20 (2018) 700–721, https://doi.org/10.1021/acscombsci.8b00113.

[23] T. Nasr, S. Bondock, M. Youns, Anticancer activity of new coumarin substituted hydrazide-hydrazone derivatives, Eur. J. Med. Chem. 76 (2014) 539–548, https://doi.org/10.1016/j.ejmech.2014.02.026.

[24] D. Rudavath, R. Sreenivasulu, S.R. Pinapati, R.R. Raju, Synthesis and anticancer evaluation of indazole-aryl hydrazide-hydrazone derivatives, J. Ind. Chem. Soc. 95 (2018) 433–438.

[25] E.M. Samir, R.M. Mohareb, Novel synthesis of pyran-3-hydrazide derivatives and their uses to the synthesis hydrazide-hydrazone, pyrazole and thiazole derivatives with anticancer activities, Bull. Chem. Soc. Ethiop. 35 (2021) 573–586, https://doi.org/10.4314/bcse.v35i3.9.

[26] I. Shabeeb, L. Al-Essa, M. Shtaiwi, E. Al-Shalabi, E. Younes, R. Okasha, M. Abu Sini, New hydrazide-hydrazone derivatives of quinoline 3-carboxylic acid hydrazide: synthesis, theoretical modeling and antibacterial evaluation, Lett. Org. Chem. 16 (2019) 430–436, https://doi.org/10.2174/1570178616666181227122326.

[27] S. Verma, S. Lal, R. Narang, K. Sudhakar, Quinoline hydrazide/hydrazone derivatives: recent insights on antibacterial activity and mechanism of action, Chem. Med. Chem. 18 (2023) e202200571, https://doi.org/10.1002/cmdc.202200571.

[28] Y. Teneva, R. Simeonova, V. Valcheva, V.T. Angelova, Recent advances in anti-tuberculosis drug discovery based on hydrazide-hydrazone and thiadiazole derivatives targeting InhA, Pharmaceuticals 16 (2023) 484, https://doi.org/10.3390/ph16040484.

[29] G. Gurkok, T. Coban, S. Suzen, Melatonin analogue new indole hydrazide/hydrazone derivatives with antioxidant behavior: synthesis and structure-activity relationships, J. Enzyme Inhib. Med. Chem. 24 (2009) 506–515, https://doi.org/10.1080/14756360802218516.

[30] A.D. Yilmaz, T. Coban, S. Suzen, Synthesis and antioxidant activity evaluations of melatonin-based analogue indole-hydrazide/hydrazone derivatives, J. Enzyme Inhib. Med. Chem. 27 (2012) 428–436, https://doi.org/10.1186/1753-6561-6-S4-P28.

[31] Ö. Aslanhan, E. Kalay, F.S. Tokalı, Z. Can, E. Şahin, Design, synthesis, antioxidant and anticholinesterase activities of novel isonicotinic hydrazide-hydrazone derivatives, J. Mol. Struct. 1279 (2023) 135037, https://doi.org/10.1016/j.molstruc.2023.135037.

[32] F.S. Tokalı, P. Taslimi, T. Taskin-Tok, A. Karakuş, N. Sadeghian, İ. Gülçin, Novel hydrazones derived from anthranilic acid as potent cholinesterases and α-glycosidase inhibitors: synthesis, characterization, and biological effects, J. Biochem. Mol. Toxicol. 38 (2024) e23521, https://doi.org/10.1002/jbt.23521.

[33] F.S. Tokalı, H. Şenol, Ş. Bulut, E. Hacıosmanoğlu-Aldoğan, Synthesis, characterization and molecular docking studies of highly selective new hydrazone derivatives of anthranilic acid and their ring closure analogue Quinazolin-4(3H)-ones against lung cancer cells A549, J. Mol. Struct. 1282 (2023) 135176, https://doi.org/10.1016/j.molstruc.2023.135176.

[34] H. Şenol, Z. Çağman, T.G. Katmerlikaya, F.S. Tokalı, New anthranilic acid hydrazones as fenamate isosteres: synthesis, characterization, molecular docking, dynamics & in silico adme, *in vitro* anti-inflammatory and anti-cancer activity studies, Chem. Biodivers. 20 (2023) e202300773, https://doi.org/10.1002/cbdv.202300773.

[35] N.N. El-Sayed, A.M. Alafeefy, M.A. Bakht, V.H. Masand, A. Aldalbahi, N. Chen, C. Fan, A. Ben Bacha, Synthesis, antiphospholipase $a_2$, antiprotease, antibacterial evaluation and molecular docking analysis of certain novel hydrazones, Molecules 21 (2016) 1664, https://doi.org/10.3390/molecules21121664.

[36] P.H.M. Torres, A.C.R. Sodero, P. Jofily, F.P. Silva-Jr, Key topics in molecular docking for drug design, Int. J. Mol. Sci. 20 (2019) 4574, https://doi.org/10.3390/ijms20184574.

[37] N. Kılınç, M. Açar, S. Tuncay, F.Ö. Karasakal, Identification of potential inhibitors for severe acute respiratory syndrome-related coronavirus 2 (SARS-CoV-2) angiotensin-converting enzyme 2 and the main protease from anatolian traditional plants, Lett. Drug. Des. Discov. 19 (2022) 996–1006, https://doi.org/10.2174/1570180819666211230123145.

[38] C.A. Lipinski, F. Lombardo, B.W. Dominy, P.J. Feeney, Experimental and computational approaches to estimate solubility and permeability in drug discovery and development settings, Adv. Drug Deliv. Rev. 23 (1997) 3–25, https://doi.org/10.1016/S0169-409X(96)00423-1.

[39] W.L. Jorgensen, E.M. Duffy, Prediction of drug solubility from structure, Adv. Drug Deliv. Rev. 54 (2002) 355–366, https://doi.org/10.1016/s0169-409x(02)00008-x.

[40] F.S. Tokalı, P. Taslimi, N. Sadeghian, T. Taskin-Tok, İ. Gülçin, Synthesis, characterization, bioactivity impacts of new anthranilic acid hydrazones containing aryl sulfonate moiety as fenamate isosteres, ChemistrySelect 8 (2023) e202300241. https://doi.org/10.1002/slct.202300241.

[41] F.S. Tokalı, H. Şenol, H.İ. Yetke, E. Hacıosmanoğlu-Aldoğan, Novel quinazoline–chromene hybrids as anticancer agents: synthesis, biological activity, molecular docking, dynamics and ADME studies, Arch. Pharm. (2023) e202300423, https://doi.org/10.1002/ardp.202300423.

[42] H. Şenol, A.G. Ağgül, S. Atasoy, Synthesis, characterization, molecular docking and invitro biological studies of thiazolidin-4-one derivatives as anti-breast-cancer agents, ChemistrySelect 8 (2023) e202300481, https://doi.org/10.1002/slct.202300481.

[43] H. Şenol, M. Ghaffari-Moghaddam, G.Ö. Alim Toraman, U. Güller, Novel chalcone derivatives of ursolic acid as acetylcholinesterase inhibitors: synthesis, characterization, biological activity, ADME prediction, molecular docking and molecular dynamics studies, J. Mol. Struct. 1295 (2024) 136804, https://doi.org/10.1016/j.molstruc.2023.136804.